SYNCHRONOUS ELECTRON BEAM DIAGNOSTIC FOR PLASMA ETCHING DISCHARGES

by

C. P. Chang and M. A. Lieberman

Memorandum No. UCB/ERL M85/38

6 May 1985

SYNCHRONOUS ELECTRON BEAM DIAGNOSTIC FOR PLASMA ETCHING DISCHARGES

by

C. P. Chang and M. A. Lieberman

Memorandum No. UCB/ERL M85/38

6 May 1985

ELECTRONICS RESEARCH LABORATORY

College of Engineering
University of California, Berkeley
94720

Synchronous Electron Beam Diagnostic for Plasma Etching Discharges*

C. P. Chang and M. A. Lieberman

Department of Electrical Engineering and Computer Sciences
and the Electronics Research Laboratory
University of California, Berkeley, CA 94720

Abstract

A synchronous electron beam diagnostic is proposed here to make local measurements on the plasma potential and the neutral density for plasma etching processes. The diagnostic utilizes an intensity-modulated monoenergetic electron beam which excites local neutral line radiation. A system consisting of lenses, optical fibers, and a photon detector is proposed to detect the amplitude and the phase of the photon signal. Frequency synchronism is used to filter out the unwanted background noise. The local neutral density is obtained from the amplitude information. The local phase information gives the plasma potential. Numerical estimates are presented for a hypothetical system with typical plasma and neutral parameters. Various potential difficulties and a calibration method are also discussed.

*Research sponsored by National Science Foundation Grant ECS-8104561.

Table of Contents

A. Introduction

Local measurements of electric field and neutral species density are always desirable in discharge monitoring for plasma etching, especially if uniformity is important. However diagnostics for accurate local measurements have not been realized. In this report we describe an electron beam time-of-flight measurement of plasma potential in the Berkeley Multiple Mirror Experiment (MMX), and we examine the feasibility of using the technique to measure local plasma potential and neutral density in plasma etching machines.

The measurement is performed by propagating a series of electron beam pulses from one side of the discharge chamber to the other (see Fig. 1). The beam electrons slow down or speed up as they move into regions of negative or positive plasma potential, respectively. By observing the time-of-flight of the beam pulses between two nearby detecting stations, the beam velocity, and thus the corresponding plasma potential, can be determined.

The amplitude of the light signal of a selected wavelength is proportional to the density of a particular neutral species, the excitation cross section, the beam intensity, and the solid angle of the detector. Thus the neutral density can be determined if the other factors are known.

For the actual measurements on the MMX that we report here (see Sec. B), a negative barrier potential is created in one mirror cell of the MMX by short pulse, electron cyclotron resonance heating (ECRH). This barrier is subsequently destroyed on the timescale for passing ions to become trapped in the heated cell. The timescale is 30-50 μsec for $T_i = T_e \approx 12$ eV, $T_h \approx 1$ keV, $n \approx 5 \times 10^{11}\text{cm}^{-3}$ typical in the MMX. The time-of-flight measurement we have developed has been used to make detailed measurements of barrier potential for a single MMX discharge on timescales as short as 5 μ sec with a potential resolution as small as $\pm$ 5 volts. The measurements are corroborated by a

number of additional diagnostics.

In the MMX, the time-of-flight is measured by means of a collector probe physically inserted into the plasma so as to intercept the beam current. The signal on plasma etching machines can be remotely sensed, so that the perturbation on the plasma is minute. In Section C, we examine a remote sensing technique which is illustrated in Fig. 1: the beam excites neutrals, yielding optical line radiation. For this technique, sources of noise exist, and signal averaging methods must be used to increase the signal-to-noise ratio. For a given time resolution, the extraction of the signal from the noise sets a limit on the use of the time-of-flight measurement. In Section C we also examine the noise sources and the required signal averaging methods. We estimate the rms uncertainty on the measured potential and neutral density due to the noise, and give the scaling of this uncertainty with the plasma and beam parameters. We give numerical estimates of plasma and beam parameters to illustrate the feasibility of the remote sensing technique. In Section D, we also examine some potential difficulties and consider their importance to the measurement techniques.

Our results are as follows: the optical line radiation technique appears feasible in most plasma etching machines. Good accuracy can be obtained on a system using a 5 kV electron beam, 0.1 torr total pressure and 0.01 torr partial pressure of active species atoms.

Of potential difficulties, beam attenuation is important when the total pressure exceeds 0.1 torr. However, a spectrum normalization using argon, sometimes called actinography, can serve as a calibration of all the uncertainties. Also differential pumping is necessary to operate a typical electron gun.

B. Potential Barrier Measurements in the MMX

A negative electrostatic potential barrier has been created in one mirror cell of a multiple magnetic mirror plasma experiment (MMX) by means of electron cyclotron resonance heating (ECRH). The potential during the formation and destruction of the barrier has been measured using an electron beam time-of-flight diagnostic, with a resolution of ± 5 volts on a 5 microsecond timescale.

The measurements are performed in the system (MMX) shown in Fig. 2. The magnetic field is pulsed, with a rise time 200 μ sec and a decay time of 2 msec. Plasma injected from a Marshall gun source flows along a 225 cm, 0.18 T, axial magnetic field and through a mirror-quadrupole field at T_8 into three cells with midplanes at M_{56}, M_{67}, and M_{78}. Each cell has length l = 75 cm and midplane field at T_6 and T_7 having mirror ratio R = 2.8 and fan ellipticity Q ≈ 20.

The 10 cm diameter metal chamber wall of the central cell, together with mesh-covered endplates at T_6 and T_7 having openings shaped to fit the elliptical flux surfaces, form a cavity for ECRH that does not obstruct the plasma flow. A 3 μ sec, 250 kW, 9.0 GHz, rf heating pulse is injected into the plasma-filled cavity at M_{67}. This creates a magnetically confined, hot electron density n_h in the center cell due to ECRH at the two resonance zones, each 6 cm from the mirror throats.

The sudden appearance of the hot-electron population, and the corresponding reduction of the cold-electron population, initiates formation of a negative potential barrier near throats T_6 and T_7 as follows: the potential V_7 of midplane M_{67} with respect to midplane M_{78} is related to the cold (non-magnetically confined) electron densities n_{67} and n_{78} by the Boltzmann relation. If $n_{67} < n_{78}$, a negative potential barrier forms near T_7:

$$V_7 = - T_c \ln (n_{78}/n_{67}), \tag{1}$$

where T_c is the cold-electron temperature. A similar expression determines V_5. These expressions are invalid in the limit $n_{67} \to 0$, where the ion flow dynamics must be considered. For this case, the potentials can be estimated by equating the total ion flux to the total electron flux entering the center cell. We obtain

$$V_7 = T_c \left[ln(1 + \frac{n_{56}}{n_{78}}) - \frac{1}{2} - \frac{1}{2} ln(\frac{2m_i}{\pi m}) \right] , \qquad (2)$$

where m_i and m are the ion and electron masses. A similar expression holds for V_6. For hydrogen ions with $n_{56} = n_{78}$, we find

$$V_7 = V_6 \approx -3.8 T_c . \qquad (3)$$

The potential barrier is destroyed on the timescale for ions to enter into and become trapped in the center cell. By quasi-neutrality, cold electrons accompany the trapped ions, and therefore n_{67} increases on the ion trapping timescale. The final state in this idealized model ($n_{56} = n_h = n_{78}$ = const and T_c = const, initially) is $n_{67} = n_h$ and $V_6 = V_7 = 0$. The total electron density (hot + cold) rises to twice its initial value after barrier destruction. Non-ideal effects important in the experiment include: initial axial density variations, non-zero ion transit time, heating of cold electrons by hot electrons, and plasma loss processes during barrier formation and decay.

The electron beam probe system, illustrated in Fig. 3, consists of an electron gun located at M_{78} and a beam collector M_{56}. The electron gun generates an electron beam having current $I_b \approx 100$ μA and voltage V_b = 150 - 200 V that propagates along the magnetic axis to the collector. The gun consists of a tungsten filament and grid located inside a 0.32 cm diameter, stainless steel tube. A 0.32 cm diameter, mesh-covered hole in the side of the tube serves as the gun anode. The beam collector is identical in construction, with the filament replaced by a collector plate.

To determine beam time-of-flight, the beam current is modulated at $f = 10$ MHz, and the phase delay of the signal received at the collector is measured. To provide high signal-to-noise ratio, a digital, phase-locked loop is used. The beam modulation is synchronized to a 100 MHz transient digitizer, and the received current, after passing through a tuned amplifier ($v_{out} = 4 \times 10^4 i_{in}$, $f = 10$ MHz, $\Delta f \approx 1.3$ MHz), is digitized. The 32 k samples are processed subsequently as follows: A sine wave is fitted to each group of twenty consecutive samples, and its amplitude A_j and phase φ_j are determined by a least square error criterion. Tens of consecutive values of sin φ_j (and cos φ_j) so determined are then averaged to obtain the mean phase φ and its standard deviation s over the five or ten microsecond sampling interval. It is easily seen that the standard deviation for a set of phases φ_j chosen randomly from the interval (0,2 π) is $\pi/\sqrt{3}$. Thus measured phases must have $s \ll \pi/\sqrt{3}$ to be considered significant; in practice, we require $s \leq 0.8$.

The phase φ (x) due to an axial potential distribution $V(x)$, with respect to the beam cathode at $x = 0$, is given by

$$\varphi(x) = \omega t(x) = \omega \int_0^x \frac{dx}{v(x)} \tag{4}$$

where

$$v(x) = \left[\frac{2eV(x)}{m} \right]^{1/2}$$

is the beam velocity. If we assume a simple square well model for the potential (see Fig. 4), then the phase change $\Delta\varphi$ at $x = 2l$ due to the creation of a negative barrier of magnitude Φ_{bar} and length l is

$$\Delta\varphi = \frac{\omega l}{v_b} \left[\left[1 - \frac{\Phi_{bar}}{V_b} \right]^{-1/2} - 1 \right] . \tag{5}$$

For $\Phi_{bar} \ll V_b$, we find

$$\Delta\varphi \approx \frac{1}{2} \frac{\omega l}{v_b} \frac{\Phi_{bar}}{V_b} . \qquad (6)$$

Fig. 5 shows the behavior of the phase delay $\Delta\varphi$ versus time after the data reduction to increase the signal-to-noise ratio. The phase is constant before ECRH, and abruptly increases by about 1.2 radians after heating. Using (5), this increase corresponds to a barrier $\Phi_{bar} \approx$ 65 V. The standard deviations s of the reduced data are small except during the first 10-20 μsec after ECRH, when the noise from the pulsed magnetron power supply and/or the sudden plasma heating dominates. After the initial phase delay, the phase change returns toward its initial value on a 50 μsec time scale. The comparison between experimental results and numerical model is given in Ref. 1.

C. Optical Line Remote Sensing Technique

1. Basic Principle and Systems

The emission rate of a particular photon wavelength due to a monoenergetic electron beam interacting with neutrals is given by

$$R(x) = n_a(x) n_b \sigma_b v_b . \qquad (7)$$

where $n_a(x)$ is the density of the neutral species that emits the photons at location x, n_b is the beam electron density, σ_b is the cross section of the reaction and is a function of v_b, and v_b is the velocity of the beam. Knowing n_b, σ_b, and v_b, we can, in principle, obtain $n_a(x)$ with determination of $R(x)$ by optical emission spectroscopy. However, accurate electron-neutral cross sections are often not available. That, plus the uncertainties in optics effectiveness, detector efficiency, and various losses make the accuracy of the determination no better than one order of magnitude. It is possible to use an inert gas as an actinometer[2,3] to reduce all the uncertainties except the cross sections. In this case, an accuracy better than a factor of two is not unreasonable. Local relative

densities can be obtained with very good accuracy.

One major problem of the electron beam diagnostic scheme is that the background emission due to interactions between the neutrals and plasma electrons is often much stronger than the beam-induced emission. In order to discriminate against the background emission, a synchronous detection technique must be used. The Synchronous Electron Beam Diagnostic (SEBD), described in this section, can distinguish the desired signal from background noise as well as provide the amplitude and phase information of the signal. The phase information, as described in Section B, can be used to determine the average plasma potential.

Figure 6 is an illustration of the basic system of an SEBD used on a parallel plate reactive ion etching (RIE) machine. The electrons are emitted, current-modulated, and accelerated in an electron gun outside the etching chamber. The beam is then injected into the chamber through an accessory port on the chamber wall. As the beam traverses the plasma, an optical signal is emitted along its path. This signal is also modulated due to the modulation of the beam. An array of fiber optical assemblies[4] (Fig. 7) located on the ground electrode, serve as detectors of the modulated signal.

Detection assemblies can either the inserted into the plasma, as shown in Fig. 6, or they can be flush, or even countersunk into the ground electrode. Each option has its merits as well as its drawbacks, as we will discuss in Section C.3. In order to increase the strength of the detected signal, each assembly has a focussing lens attached to the end of each fiber.

Since almost all plasma etching processes are operated nearly steady state, fast time resolution is not necessary. A switching mechanism is proposed here to utilize only one photon detector for all detection assemblies. For a fixed period of time, the signal from only one fiber is sent to the detector, and subse-

quently analyzed. The data from the digitizer is first averaged. Since the signal modulation is synchronous with the sampling rate the averaging will not affect the true signal, but will smooth out the background fluctuations. A least square method can then be used to fit the averaged data and obtain its amplitude and phase. The amplitude can be used to calculate neutral density near the detector.

As described in Section B, the phase information can be used to determine the plasma potential between two detectors. With the distance between the beam and the powered electrode known, local electric fields, which are very important to uniformity in RIE, can be estimated.

An alternative data reduction system is shown in Fig. 8. The filtered signal is sent to a power detection diode and a phase locked detector. The output of the diode is proportional to the square of the signal amplitude, and the phase detector gives the phase shift relative to a reference signal. Good signal-to-noise ratio can be obtained by an analog averager which integrates over a number of modulation cycles. The above system does not use a digitizer and subsequent digital data processing, but provides similar signal-to-noise ratio improvement. Note that both systems can be adapted to use a background subtraction scheme; namely, we turn off the beam, and observe $\bar{A}$ and $\bar{\varphi}$ which are due to background fluctuations alone. Then we can subtract the average noise signal from the data taken with the electron beam on. In the digital system (Fig. 6), a computer program can do the subtraction. In the analog system (Fig. 8), we can adjust the dc offset of the recorder such that it reads zero when the electron beam is off.

More information can be obtained if we use a scanned beam. As shown in Fig. 9, the beam is deflected before entering the etcher by an external electric field. We can put detection assemblies over the scanned area and make local

measurements. The basic technique of an electron beam scan is well established from the design of cathode ray tubes. The application here should be straightforward.

It is apparent that there are two ways to implement SEBD. One way is by computer control. A computer controls the beam scan, photon signal switching mechanism, data acquisition, and data analysis. The whole system is automatic. Another way is to take advantage of the fact that fast time response is not needed, and control the system manually. It is also clear that by changing optical filters or adjusting a monochrometer, the system can be used to monitor densities of more than one neutral species. Again this option can be selected manually or automatically.

Measurement Technique

In this section we present quantitatively the measurement technique and obtain expressions for the mean electrostatic potential $\overline{V}$ and mean amplitude s_0 as well as their root mean square deviation. We consider the process of electron beam excitation of optical line radiation from neutral gas atoms. We let

n_a = neutral atom density (cm^{-3})

n_b = electron beam density (cm^{-3})

n_e = electron beam density (cm^{-3})

$< \sigma v >_b$ = beam-atom excitation rate(cm^3/sec)

$< \sigma v >_e$ = plasma electron-atom excitation rate(cm^3/sec)

Δ_b = beam-neutral interaction volume(cm^3)

Δ_e = plasma electron-neutral interaction volume(cm^3)

Roughly, we estimate (see Fig. 7) that

$$\Delta_b = \pi r_b^2 l \ ,$$

and

$$\Delta_e = 2 r_b d_e l \ ,$$

where r_b and d_e are respectively the beam radius and the plate separation, and l is the interaction length. Then the photon generation rates for the beam and for the plasma electrons are, respectively,

$$R_b = n_a n_b \sigma_b v_b \Delta_b, (\text{photons/sec}) \tag{8}$$

$$R_e = n_a n_e <\sigma v>_e \Delta_e, (\text{photons/sec}) \tag{9}$$

Now we let

f = beam density modulation frequency (Hz),

Ω = solid angle seen by the optics (steradians),

J = number of sample intervals per modulation period,

M = number of modulation cycles.

The observation time interval; i.e., the time resolution of the measurement, is

$$T = M/f.$$

We have divided each modulation period $\tau = 1/f$ into J equal subintervals $\Delta t = \tau/J$. There are thus three time scales: $\Delta t, \tau$ and T.

During a period τ, we observe within each subinterval Δt

$$N_b = \eta R_b \ \frac{\Omega}{4\pi} \Delta t \quad (\text{photons}) \tag{10}$$

$$N_e = \eta R_e \ \frac{\Omega}{4\pi} \Delta t \quad (\text{photons}) \tag{11}$$

where $\eta<1$ is the detector efficiency. We consider N_b to oscillate at frequency f, while N_e will be steady (dc), with fluctuations due to photon counting

statistics. The fluctuations in N_e must be considered because N_b is very small compared to N_e. (Note that $n_b \ll n_e$ and $\Delta_b < \Delta_e$.) We must use averaging techniques to increase the signal-to-noise ratio of the measurement. Since N_e has a large dc component, we use a band-pass filter to subtract that from the signal. In this manner, the photon baseline for the noise is subtracted, leaving only its fluctuation level.

Taking M samples for each subinterval j (one sample during each modulation period as shown in Fig. 10), we obtain the rms fluctuation level (noise)

$$F_{rms} = (MN_e)^{1/2} \text{(photons)} \tag{12}$$

The signal is present for half the samples, yielding

$$S_j = \frac{1}{2} MN_b(t_j) \quad \text{(photons)}, \tag{13}$$

where t_j (modulo τ) is the subinterval time. Since $N_b \ll N_e$, the fluctuations in S_j are not important. The signal-to-noise ratio is defined as

$$S_j / F = \frac{1}{2} \frac{N_b}{N_e^{1/2}} M^{1/2}, \tag{14}$$

and increases as the square root of the number of samples taken. The output signal from the detector, after averaging, is the set of J values

$$P_j = S_j + F_j \quad \text{(photons)}, \tag{15}$$

where F_j is the number of noise photons in the jth subinterval.

We now determine the phase φ from the values of P_j, and estimate the rms phase uncertainty $(\Delta\varphi)_{rms}$. For simplicity we assume that the signal, uncorrupted by noise, has the form

$$S(t) = S_0 \sin(\omega t + \varphi_0), \tag{16}$$

where $\omega = 2\pi f$, and S_0 and φ_0 are the amplitude and phase to be determined. (It is easy to add a constant term to S if required).

To determine the "best fit" values of S_0 and φ_0, we minimize the mean squared error

$$e = \sum_{j=1}^{J} (S(t_j) - P_j)^2 \Delta t \ . \tag{17}$$

Setting $\partial e / \partial \varphi_0$ and $\partial e / \partial S_0 = 0$, we obtain the two equations

$$\sum_j P_j \cos(\omega t_j + \overline{\varphi}) = 0 \tag{18}$$

$$\overline{S} = \frac{2}{J} \sum_j P_j \sin(\omega t_j + \overline{\varphi}). \tag{19}$$

Equation (18) determines the "best fit" phase $\overline{\varphi}$, and (19) yields the "best fit" amplitude $\overline{S}$.

The uncertainty in $\overline{\varphi}$ can be found by inserting (16) into (18):

$$\sum_j S_0 \sin(\omega t_j + \overline{\varphi}) + \sum_j F_j \cos(\omega t_j + \overline{\varphi}) + \sum_j F_j \cos(\omega t_j + \overline{\varphi}) = 0 \tag{20}$$

We assume that $\overline{\varphi}$ is close to φ_0 and that the F_j's are small. We thus put $\overline{\varphi} = \varphi_0$ in the second term in (20), and put

$$\overline{\varphi} = \varphi_0 + \Delta\varphi; \quad \Delta\varphi \ll 2\pi$$

in the first term. We than obtain the relation

$$S_0 \frac{J}{2} \Delta\varphi = \sum_j F_j \cos(\omega t_j + \varphi_0). \tag{21}$$

Recall that the F_j are Gaussian-distributed random variables, having $\overline{F_j} = 0$ and $\overline{F_j^2} = F_{rms}^2$.

Averaging over this distribution, we obtain $\overline{\Delta\varphi} = 0$ and

$$\overline{(\Delta\varphi)^2} = (\Delta\varphi_{rms})^2 = \frac{2}{J} \frac{F_{rms}^2}{S_0^2}. \tag{22}$$

Using (8)-(13), we obtain

$$(\Delta\varphi_{rms})^2 = \frac{8}{N_T}\frac{n_e}{n_{bmax}}\frac{<\sigma v>_e}{\sigma_b v_b}\frac{\Delta_e}{\Delta_b} \tag{23}$$

where

$$N_T = \eta\frac{\Omega}{4\pi} n_a n_{bmax}\ \sigma_b v_b \Delta_b T \tag{24}$$

is the total number of beam photons that would be detected during a time interval T if the beam density was n_{bmax} during the entire interval. As expected, we note that $\Delta\varphi_{rms}$ depends only on the averaging time T, and not on τ or Δt. If we insert (16) into (19), make the same assumptions as in (20), and put

$$\overline{S} = S_0 + \Delta S; \quad \Delta S \ll S_0$$

in left hand side of (19), we then obtain

$$\Delta S = \frac{2}{J}\sum_j F_j \sin(\omega t_j + \varphi_0). \tag{25}$$

If we define the relative amplitude variance by

$$(\Delta S^*_{rms})^2 \equiv \frac{(\Delta S_{rms})^2}{S_0^2}, \tag{26}$$

then follow the same procedure as from (21) to (22) to obtain

$$\overline{\Delta S} = 0,$$

$$(\Delta S^*_{rms})^2 = \frac{2}{J}\frac{F^2_{rms}}{S_0^2} = (\Delta\varphi_{rms})^2. \tag{27}$$

The fluctuation in neutral density Δn_a due to the fluctuation ΔS_{rms} of the amplitude is easily obtained:

$$\Delta n^*_{rms} \equiv \frac{\Delta n_{arms}}{n_a}$$

$$\Delta n^*_{rms} = \Delta S^*_{rms} = \Delta\varphi_{rms} \tag{28}$$

We now relate the mean potential $\overline{V}$ and its rms deviation ΔV_{rms} to the mean phase $\overline{\varphi}$ and its rms deviation $\Delta\varphi_{rms}$. The phase is given in terms of the potential by the equation

$$\varphi(x) = \omega t(x) = \omega(\frac{m}{2e})^{1/2}\int^{x} dx' [V(x')]^{-1/2}, \tag{29}$$

where $V(x)$ is the potential with respect to the electron beam cathode. Solving for V, we obtain

$$V(x) = \frac{m\omega^2}{2e}[\varphi'(x)]^{-2}, \tag{30}$$

where

$$\varphi' = d\varphi/dx.$$

We use the values of φ obtained at two axial locations (see Fig. 1) to determine φ':

$$\varphi' = \frac{\varphi_2-\varphi_1}{\Delta L}, \tag{31}$$

where ΔL is the axial separation. We note that φ' has the mean

$$\overline{\varphi}' = \frac{\overline{\varphi}_2-\overline{\varphi}_1}{\Delta L} \tag{32}$$

and the rms deviation

$$\Delta\varphi'_{rms} = \frac{\sqrt{2}\Delta\varphi_{rms}}{\Delta L}. \tag{33}$$

Thus V has the mean

$$\overline{V} = \frac{m\omega^2}{2e(\overline{\varphi}')^2} \tag{34}$$

and the rms deviation

$$\Delta V_{rms} = \frac{m\omega^2}{e(\overline{\varphi}')^3}\Delta\varphi'_{rms}. \tag{35}$$

Inserting (33) and (34) into (35), we obtain

$$\Delta V_{rms} = \frac{4}{\omega}\left(\frac{e}{m}\right)^{1/2}\overline{V}^{3/2}\,\frac{\Delta\varphi_{rms}}{\Delta L}$$
$$= A_v\,\frac{\overline{V}^{3/2}}{f\,\Delta L}\Delta\varphi_{rms} \qquad (36)$$

where

$$A_v = 2.7\times10^5\ \mathrm{m/V^{1/2}\text{-}sec.}$$

For design of the electron beam probe diagnostic system, we should therefore choose $f, \eta, \omega, l, \Delta L$, and T as large as possible, and choose V_b as small as possible (we assume here that $\sigma_b v_b$ is roughly independent of v_b).

3. Practical Considerations and Numerical Estimates

To achieve smaller values of $\Delta\varphi_{rms}$, a low electron beam velocity v_b is desirable. However, the mean free path for elastic scattering of a 300 eV electron beam is shorter than that of a 10 keV electron. The lower energy beam suffers more attenuation and divergence. Furthermore, the lower energy beam is more efficient at ionizing neutrals, and the resulting energy loss is significant. Typically for 300 eV electrons, the ionization cross section is $\sigma_i \approx 10^{-16}\mathrm{cm}^2$, and the energy loss is $\Delta E_i \approx 30$ eV/ionization. If the neutral pressure p is 0.1 torr, the beam energy loss is 10 eV/cm which is too high for a system typically 30 cm long. However, for low pressures ($p \ll 0.1$ torr), a 300 eV beam seems feasible and may be a better choice than a higher energy beam.

The upper bound on the modulation frequency f is set by the transition time for the line radiation. Typically, the transition rate is on the order of 60 MHz for atoms like hydrogen. A lower bound for f is determined by $\Delta\varphi_{rms}$. For a phase difference measurement to be considered good, we must have

$$\varphi_2 - \varphi_1 > \Delta\varphi_{rms} \tag{37}$$

Since

$$\varphi_2 - \varphi_1 \approx 2\pi f \frac{\Delta L}{v_b},$$

the lower bound is given by

$$f > \frac{v_b \Delta\varphi_{rms}}{2\pi\Delta L} . \tag{38}$$

Another restriction on the modulation frequency is that the phase shift difference has to be greater than the phase error $\Delta\varphi_s$ due to the digitizing error and the modulation error (not a perfect sinusoid). Typically, this type of phase error is on the order of 0.01 rad. on the diagnostic system used on MMX. For a different system, a test should be made to determine $\Delta\varphi_s$. In order to obtain an accurate phase difference,

$$f > \frac{v_b}{2\pi} \frac{\Delta\varphi_s}{\Delta L} . \tag{39}$$

The spatial resolution of the measurement is directly related to ΔL. For a good spatial resolution, ΔL has to be small. However, for a fixed f, (39) sets a low bound on ΔL. Furthermore, a decrease of ΔL results in an increase in the total number of optical detectors which results in more expense and complications in the switching mechanism. A compromise is necessary.

In order to achieve good spatial resolution and adequate signal-to-noise ratio, a highly focussed beam is desirable. That is, the current intensity j_b (A/cm^2) should be high, and r_b should be small. However, even without the broadening effect due to collisions with neutrals, the focussing is limited by the space charge effects within the beam. From Poisson's equation

$$\frac{E_\perp}{r_b} \sim \frac{n_b e}{\varepsilon_0} ;$$

where $E_\perp$ is the transverse electric field, e is the electron charge, and ε_0 is the vacuum permittivity. Since

$$n_b e = \frac{I_b}{\pi r_b^2 v_b},$$

we obtain

$$E_\perp \sim \frac{I_b}{\pi \varepsilon_0 v_b r_b}. \tag{40}$$

The field $E_\perp$ tends to expand the beam radius. A rough estimation can be made by approximating the transverse acceleration as $a_\perp \sim \frac{eE_\perp}{m}$. Then the maximum beam radius increase, after travelling a distance L, is

$$\delta_{max} \approx \frac{1}{2}\frac{eE_\perp}{m}\left(\frac{L}{v_b}\right)^2 = \frac{1}{2}\frac{eI_b L^2}{\pi \varepsilon_0 m v_b^3 r_b}. \tag{41}$$

Note that (41) is valid only when $\delta \ll r_b$. In reality, a better estimation is $\delta \approx \delta_{max}/3$. Furthermore, (41) is not applicable to a neutralized electron beam. In the discharge region, the plasma could provide enough background ions to neutralize the electron beam, in which case, the electron beam radius does not expand. As long as the beam electron density is much lower than the plasma electron density, the neutralization would not affect the plasma potential either locally or globally.

In order not to disturb the discharge characteristics, the total area of the optics should be small compared to the ground electrode. This can be written as

$$N_0 A_0 \ll A_G \tag{42}$$

where N_0 is the number of detectors and A_0 is the area of a detector. A typical optical fiber has a radius of $10^2 \mu$m. In order to increase photon collection, a lens can be placed in front of the fiber. If we keep the lens size on the order of a

millimeter, (42) should be satisfied with tens of optical detectors without problem. The detection assemblies that are inserted into the system can be very close to the beam. Therefore, they inherently have better signal-to-noise ratio. It remains to be seen whether this type of assemblies will disturb the discharge. However, it is highly probable chemical reactions will take place on the surface of an inserted assembly due to the abundance of reactive species in the system. Extra efforts may have to be made to prevent corrosion. Assemblies that are flush or countersunk into the electrode are less vulnerable to corrosion, but they collect less signal emitted by beam-neutral excitations due to a smaller solid angle. For high pressure processes ($p \gtrsim 0.1$ Torr) flush assemblies are probably preferable due to the high concentration of chemically reactive species. But for low pressure processes ($p \ll 0.1$ Torr), inserted, assemblies may be necessary because of the low emission intensity.

As an example for overall consideration, we consider a system with chamber diameter L = 30 cm, electrode radius R = 12 cm, electrode separation d_s = 2 cm, overall neutral pressure p = 0.1 Torr., and partial pressure of hydrogen atoms 0.01 Torr. Hydrogen is chosen here to represent a general radical species, e.g., fluorine atoms, due to lack of cross section information for other species. The synchronous electron beam is 0.5 cm above the electrode where the etching takes place. Five fiber optical assemblies with 0.5 cm diameter size are located on the other electrode. Thus,

$$\Delta L = \frac{2R}{5-1} = 6 \text{ cm} .$$

Because the pressure is 0.1 Torr. a 5 keV electron beam is used. If we assume $\Delta\varphi_s$ is 0.01 radians, then from (39), we obtain

$$f > 1\text{MHz} .$$

we choose $f \approx 40$ MHz. The solid angle of an optical assembly is

$\Omega = 0.087$ steradians

We choose an averaging time T = 1msec. Since there is no limit on time resolution, T is limited by the capability of the data acquisition system. A beam with I_b = 0.1 A and r_b = 0.2 cm is chosen. From (41), the beam self space charge gives, when it reaches the edge of the plasma,

$\delta \approx 0.5$mm.

The beam radius expands about 25% which is acceptable. The density of beam electrons is

$$n_b = \frac{I_b}{\pi r_b^2 v_b} = 1.6\times10^9 \text{cm}^{-3}.$$

From p = 0.01 Torr, we can calculate the hydrogen density

$$n_a = 3.3\times10^{14}\text{cm}^{-3}.$$

The background electron density is roughly 10^{-4} to 10^{-6} of the total neutral density. Taking a median value of 10^{-5}, we obtain the background electron density

$$n_e \approx 3.3\times10^{10}\text{cm}^{-3}.$$

Letting $l = \Delta L$, we calculate the signal and noise volumes.

$$\Delta_b = 0.75 \text{ cm}^3$$

$$\Delta_e = 4.8 \text{ cm}^3$$

The Balmer α line cross section[5] has a threshold of 12 eV. If we assume a typical plasma electron temperature of 5 eV, and the electron distribution is a maxwellian (an overestimation at the high energy tail), we can calculate

$$< \sigma v >_e \approx 1.3\times10^{-10}\text{cm}^3/\text{sec}.$$

For 5 keV electrons, the Balmer α line cross section is

$$\sigma_b \approx 5\times10^{-19}\text{cm}^2.$$

From that, we obtain

$$\sigma_b v_b \approx 2.4\times10^{-9}\text{cm}^3/\text{sec}.$$

From (8) and (9),

$$R_b = 7.1\times10^{14}\text{photon/sec}$$

$$R_e = 6.8\times10^{15}\text{photon/sec}$$

Since $T = 10^{-3}$sec and $f \approx$ 40 MHz, then

$$M = 4\times10^{4}(\text{number of cycles averaged})$$

The photon loss in an optical fiber is typically 50 dB/km. The losses in the interface are about 0.2 dB/interface. Other losses may be about 1-2 dB. For a detection assembly 1 m long, it is reasonable to assume that about 60% of the photons collected by the lens actually enter the photo-multiplier tube. For f = 40 MHz, J = 4, using (10) and (11), we find that

$$N_{bmax} = 2.5\times10^{4}\text{photons},$$

$$N_e = 2.4\times10^{5}\text{photons}.$$

Using (12) and (13), we obtain

$$F_{rms} = 9.8\times10^{4}(\text{noise photons/subinterval})$$

$$S_{jmax} = 5.2\times10^{8}(\text{signal photons/subinterval})$$

Using (22) and (27), we obtain

$$\Delta S^{*}_{rms} = \Delta\varphi_{rms} = 1.0\times10^{-4}\ .$$

Finally using (36), we obtain the rms potential uncertainty

$$\Delta V_{rms} = 4.0\text{volts} \ .$$

Note that phase shift between two adjacent optical detectors is

$$\varphi_2 - \varphi_1 \simeq 2\pi f \frac{\Delta L}{v_b} = 0.38\text{radians} \ .$$

which satisfies both (38) and (39). From (28), we know

$$\Delta n^* = \Delta S^*_{rms} = 1.0\times10^{-4}.$$

Since we can expect to see relative local density variations on the order of 10^{-1}, an uncertainty of 1.0×10^{-4} is negligible. Since, the plasma potential ranges from 20 V to 600 V typically, a ΔV_{rms} of 4.0 V may be marginal at the low end. However, at low pressure ($p < 0.1$Torr), we can use a lower energy beam without the problem of beam divergence and attenuation. If we use a 2 keV beam in the above analysis, we obtain

$$\Delta V_{rms} = 0.9\text{V}$$

$$\varphi_2 - \varphi_1 = 0.6 \text{ radians}$$

These values are very reasonable for making an accurate measurement of the local potential.

D. Possible Difficulties

In this section we examine the possible difficulties which include (1) beam-plasma interaction; (2) beam attenuation due to collision with neutrals; (3) beam deflection due to rf and dc electric fields; and (4) pumping problems. We also use Section D.5 to discuss the calibration of the diagnostic.

1. Electron Beam-plasma Instabilities

Collective motions (waves, instabilities) are a feature of plasmas without relatively strong collisions which tend to randomize any collective effect and dis-

sipate the wave energy. For all remote detection techniques, beam-plasma instabilities may lead to dispersion in beam parallel velocity and a reduction in measured signal strength. In addition, beam phase shift may no longer be related simply to variations in plasma potential; i.e., the electron beam may slow down due to beam-plasma interactions. As a rule of thumb, if $\nu_c \sim f_p$, then collective effects are not expected to be important. Here, ν_c is the electron-neutral collision rate, and f_p is electron plasma frequency. In plasma etching processes, especially at high pressure ($p > 0.1$ torr), charged particle motion is strongly affected by collisions with neutrals. An example: Given a system with $p = 0.1$ torr, we have $n_a = 3.4\times10^{15}\text{cm}^{-3}$, and $n_e \sim 3.4\times10^{10}\text{cm}^{-3}$ ($n_e/n_a \approx 10^{-5}$). Choosing an electron temperature of 5eV, then $\sigma_c \sim 1\times10^{-15}\text{cm}^{-3}$, and $v_e \sim 2\times10^{8}\text{cm/sec}$. Using the above parameters, we obtain

$$f_p = \frac{n_e e^2}{2\pi m \varepsilon_0} \approx 1.5\times10^{9}\text{Hz},$$

and

$$\nu_c \simeq n_a \sigma_c v_e \approx 1\times10^{9}\text{Hz}.$$

Since $f_p \sim \nu_c$, beam-plasma instability is heavily damped. Note that, at lower pressure, n_e/n_a is generally lower. If we choose $p \sim 0.01\text{torr}$ and $n_e/n_a \sim 10^{-6}$, we again obtain $f_p \sim \nu_c$.

2. Beam Attenuation and Divergence

Strong collisionality gives rise to beam attenuation and divergence. We note first that the electron mean free path is

$$\lambda_{mfp} = \frac{1}{n_a \sigma_a} \tag{42}$$

For a 5 keV beam, the elastic cross section[6] is about $5\times10^{-17}\text{cm}^{-3}$. Letting

$n_a = 3.3\times10^{15}\text{cm}^{-3}$ (p = 0.1 torr), we obtain

$$\lambda_{mfp} = 5 \text{ cm}$$

Compared to a path length of 25 cm, λ_{mfp} is small, and the beam broadening effect could be significant. However, looking into the literature,[7] we find experimental evidence that there is little broadening of a high energy electron beam (20 keV, 0.1mm diameter) for $p < 0.1$ torr. Furthermore, a usable beam spot (1mm diameter) was obtained for pressures up to between 1 and 5 torr, in a 10 cm diameter tube.

If the broadening of the beam is small compared to the distance between the optical detectors and the beam, it only has a minor effect on the signal collection. However, attenuation directly affects the accuracy of the neutral density measurement. The attenuation is due to large angle scattering and ionization. It is difficult to estimate the extent of the attenuation along the path of the beam. However, the attenuation problem can be alleviated by a calibration employing an actinometer technique using, say argon. A brief discussion of actinography will be presented in Section D.5.

3. Electric Field Effects

The electron beam, when it feels an electric field perpendicular to its path, will be deflected. In plasma etching, the perpendicular electric field $E_\perp$ can be written as

$$E_\perp = E_{\perp_{dc}} + E_{rf} \quad .$$

Since the typical rf frequency is 13.6 MHz, the period $T_{rf} \approx 70$nsec. However for a 10 kV beam travelling $L =$ 30 cm, the transit time is 5 nsec. $\ll T_{rf}$. Therefore, it is safe to assume that a constant electric field is seen by an electron when it travels through the plasma. Hence

$$E_0 \equiv E_{\perp_{max}} = E_{\perp dc} + E_{rf_{max}}$$

We can calculate ΔZ, the deflection due to E_0 as follows:

$$\Delta Z = \frac{e}{m} E_0 \frac{t^2}{2}$$

Let $t_0 = \frac{L}{v_b}$; then

$$\Delta Z = \frac{1}{4} \frac{E_0}{V_b} L^2 \ . \tag{45}$$

A typical case might be $E_0 \approx$ 18 V/cm, L = 20 cm and V_b = 5 kV. Then from (45), ΔZ = 0.25 cm. The deflection of the beam will not affect the alignment between the beam and the optics, but it will slightly change the solid angle of detection (Fig. 10). Typically, $Z \sim$ 2 cm, $Z' = Z + \Delta Z$ = 2.25 cm such that

$$\frac{\Omega'}{\Omega} = \frac{Z^2}{Z'^2} = \frac{4}{5} \ .$$

Thus a 20% error is introduced, if we use the solid angle assuming no deflection. Note that by using averaging, the effect of E_{rf} can be eliminated. The effect of $E_{\perp dc}$ can not be averaged away, but a calibration with an actinometer can also help to eliminate the effect.

4. Pumping

The neutral pressure in a plasma etcher ranges from 10^{-3} torr to a few torr. An electron emitter, such as a hot filament, performs poorly at high ambient pressure. Also, to ensure proper modulation and acceleration of the beam, the electron mean free path in an electron gun should be longer than the length of the gun. For a typical gun length of 10 cm, a pressure $<10^{-3}$ torr in the gun is necessary.

For low pressure reactive ion etching processes, $p \sim 10^{-3}$torr, extra effort may not be needed for pumping. However, for high pressure processes, such as

high pressure plasma etching, differential pumping is probably needed to achieve lower pressure in the gun. We can estimate the pumping speed and the through-put needed as follows:

A typical speed for pumping[8] through a tube of length l and diameter d is

$$S = 3.81\left(\frac{T}{M}\right)\frac{d^3}{l};$$

where d(cm), l(cm), S(liter/sec), T(°K), and M(amu) is molecular weight of the gas. Typically, T = 400 °K, and M = 68 for a gas like CF_4. The through-put Q can be expressed as

$$Q(\text{liters}-\text{torr}/\text{sec}) = \Delta p\, S.$$

For a gun 10 cm in length and 1 cm in diameter, the through-put needed for differential pumping of Δp = 1 torr is

$$Q = 0.9 \text{ liter}-\text{torr}/\text{sec}$$

which is a reasonable value.

5. Calibration with Actinometer

It is clear that, as described in Sec. D.1-D.4, uncertainty due to various non-ideal effects can be significant. Furthermore, the transmission loss of the optical signal, the interface coupling loss, and the response of the photon detector can give rise to more uncertainties. A calibration with a known light emitter can partially reduce the uncertainty of the data acquisition system. However, actinography[2,3] is probably needed to eliminate the uncertainty due to the non-ideal effects.

The general practice of actinometer calibration, so called actinography, is to put a noble gas into the system and detect the optical emission due to interactions between electrons and the gas atoms. Since the gas is chemically inert, its density should be constant in time. Therefore, the emission can serve

as a reference to optical emissions by other neutral species. A reliable determination of the relative density of a desired neutral species can be obtained by simply taking the ratio between the emission intensity of the species and the reference. An absolute determination is not available, because the plasma electron distribution and the detailed cross section information are generally not known. The uncertainty in the distribution can be removed by SEBD, by virtue of using a monoenergetic electron beam. Therefore, SEBD can make an accurate local measurement of the absolute density of a desired species, provided that the cross section corresponding to the electron beam energy is available.

The calibration can be done on SEBD by adjusting the monochrometer or changing the optical filter. In order to ensure the accuracy, the calibration should be done repeatedly during the course of an etching process. The repetition rate is, of course, determined by the length of the process and the desirable time resolution.

Note that a calibration per se can provide us the phase information. Since the density of an actinometer gas is stable and can be controlled externally, it is probably best to use the calibration gas to obtain local plasma potential along with the amplitude calibration factor for the active neutral species.

Acknowledgments

The authors wish to thank Dr. A. Voshchenkov of the Bell Laboratories, Murray Hill, who first suggested the application of SEBD to non-uniformity detection in plasma etching processes. We would like to thank Dr. H. Meuth for contributing much insightful information. We are also grateful to Dr. J. W. Coburn of the IBM San Jose Research Laboratory for a useful telephone discussion with one of the authors.

References

[1] M. A. Lieberman and C. P. Chang, Electron Beam Time-of-Flight Measurements of Plasma Potential in Tandem Mirrors, University of California, Berkeley, Memorandum UCB/ERL M84/92 (1984).

[2] J. W. Coburn and M. Chen, *J. Appl. Phys.*, 51, 3134, (1980).

[3] R. d'Agostino, F. Cramarossa, S. DeBenedictis, and G. Ferraro, *J. Appl. Phys.*, 52, 1259, (1981).

[4] A. M. Voshchenkov, private communication (1984).

[5] Atomic Data for Controlled Fusion Research, Oak Ridge Nat'l. Lab., ORNL-5207 (1977).

[6] D. J. Rose and M. Clark, Jr., *Plasma and Controlled Fusion*, J. Wiley, New York, (1961).

[7] R. W. Warren, *Rev. Sci. Instr.*, 26, 765, (1955).

[8] A. Roth, *Vacuum Technology*, North-Holland, Netherlands, p. 82 (1976).

Figure Captions

Fig. 1. Remote sensing for electron beam measurements to determine the electrostatic potential $V(x)$ and the neutral densities $n_a(x)$ in a plasma etcher.

Fig. 2. Electron beam time-of-flight measurement of thermal barrier potential on the Multiple Mirror Experiment (MMX).

Fig. 3. Electron beam diagnostic setup on the MMX.

Fig. 4. Square well model for thermal barrier formation and destruction.

Fig. 5. A typical time-of-flight measurement for one experimental discharge shot; (a) raw data $v_{out}(t)$ vs t, digitized at 100 MHz sampling rate, with every other sample shown; (b) reduced data; showing beam phase delay $\Delta\varphi(t)$ vs t, with averaging over 100 rf cycles, yielding 10 μsec time resolution. The rms deviation is shown as the vertical line. The circles are points whose rms deviations exceed 0.8 radians.

Fig. 6. Synchronous Electron Beam Diagnostic (SEBD) with digital data acquisition system for an RIE etcher.

Fig. 7. Fiber optical assembly and definitions of beam and plasma interaction volumes.

Fig. 8. SEBD with an analog data processing system.

Fig. 9. Electron beam scan and scanned area.

Fig. 10. Electron beam deflection ΔZ due to an electric field in the discharge.

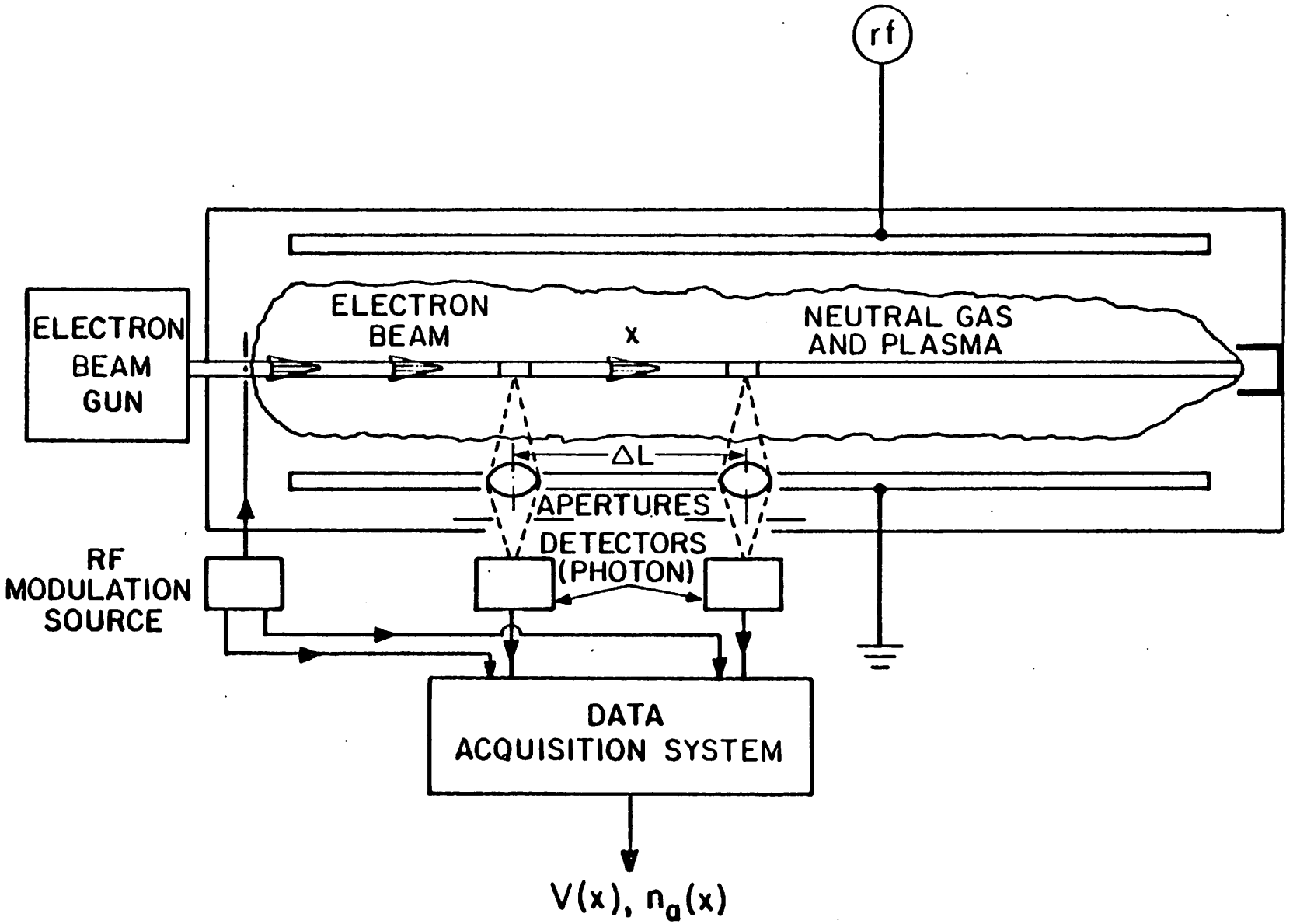
rf
ELECTRON BEAM GUN
ELECTRON BEAM
x
NEUTRAL GAS AND PLASMA
ΔL
APERTURES
DETECTORS (PHOTON)
RF MODULATION SOURCE
DATA ACQUISITION SYSTEM
V(x), n_a(x)

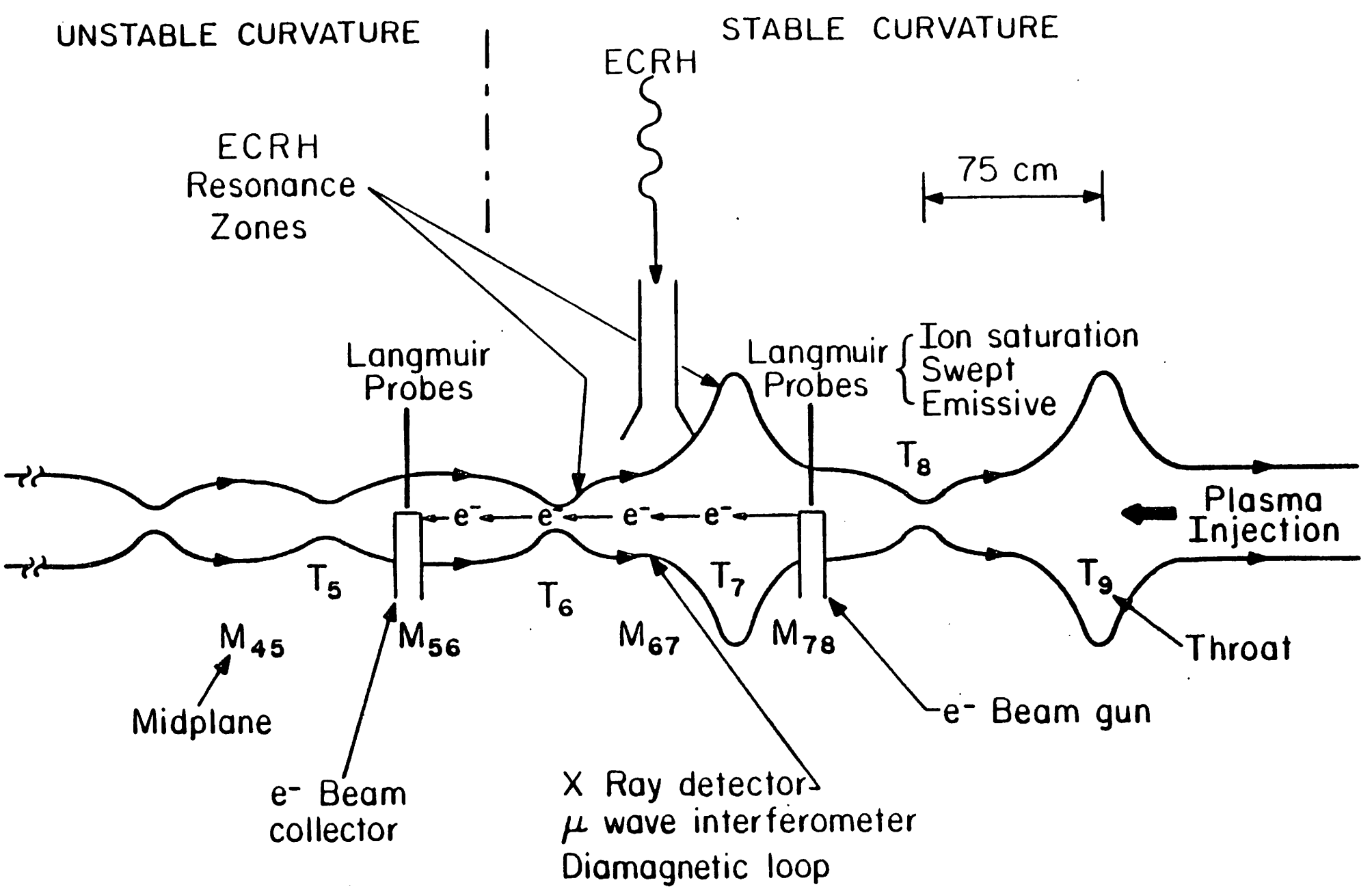
UNSTABLE CURVATURE
STABLE CURVATURE
ECRH
ECRH
Resonance
Zones
75 cm
Langmuir
Probes
Langmuir
Probes
Ion saturation
Swept
Emissive
T8
e-
e-
e-
e-
Plasma
Injection
T5
T6
T7
T9
M45
M56
M67
M78
Throat
Midplane
e- Beam gun
e- Beam
collector
X Ray detector
μ wave interferometer
Diamagnetic loop

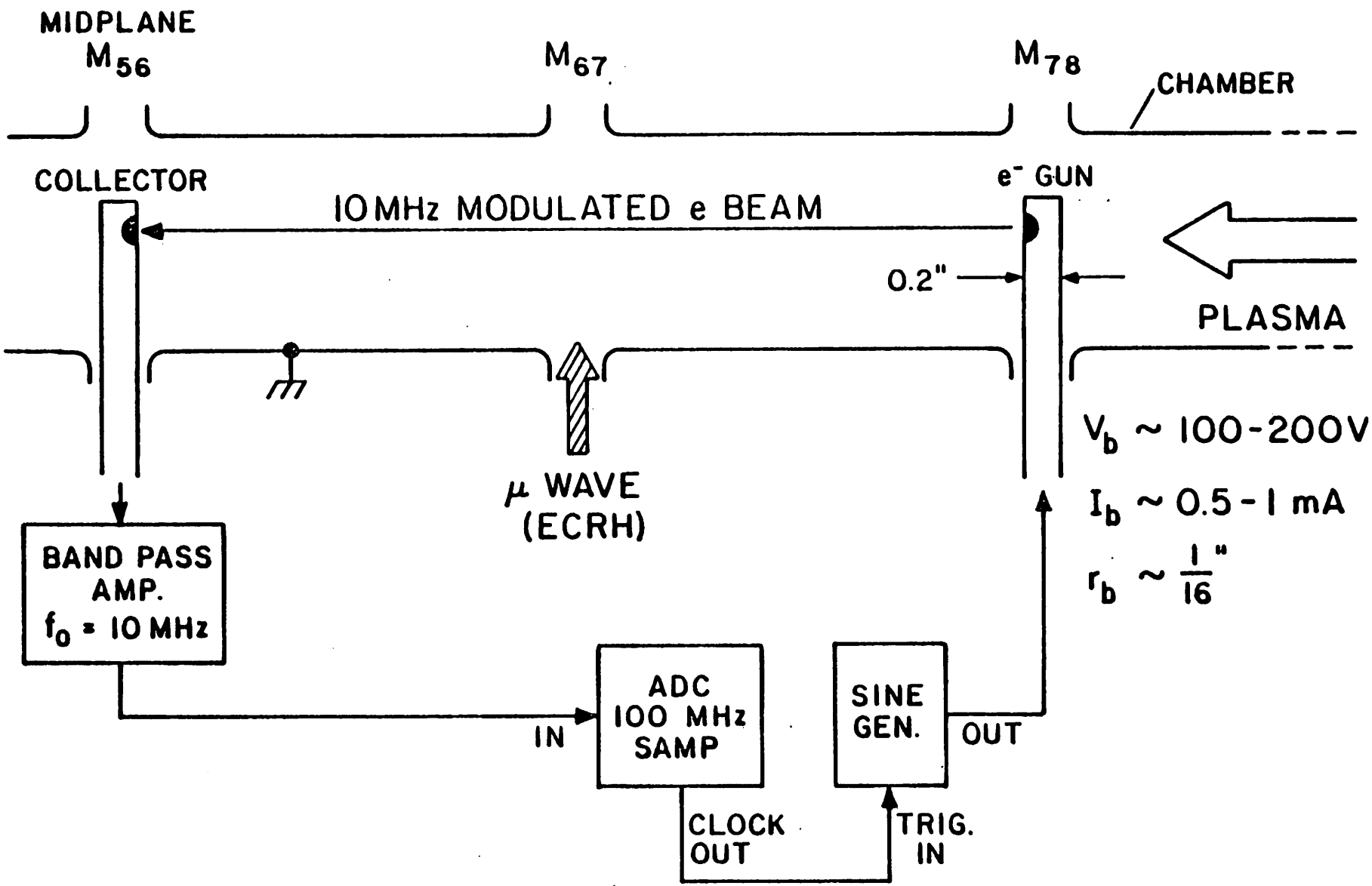
MIDPLANE
M_{56}
M_{67}
M_{78}
CHAMBER
COLLECTOR
e⁻ GUN
10 MHz MODULATED e BEAM
0.2"
PLASMA
$V_b \sim 100\text{-}200V$
$I_b \sim 0.5\text{-}1$ mA
$r_b \sim \frac{1}{16}$"
μ WAVE
(ECRH)
BAND PASS
AMP.
f_0 = 10 MHz
ADC
100 MHz
SAMP
IN
SINE
GEN.
OUT
CLOCK
OUT
TRIG.
IN

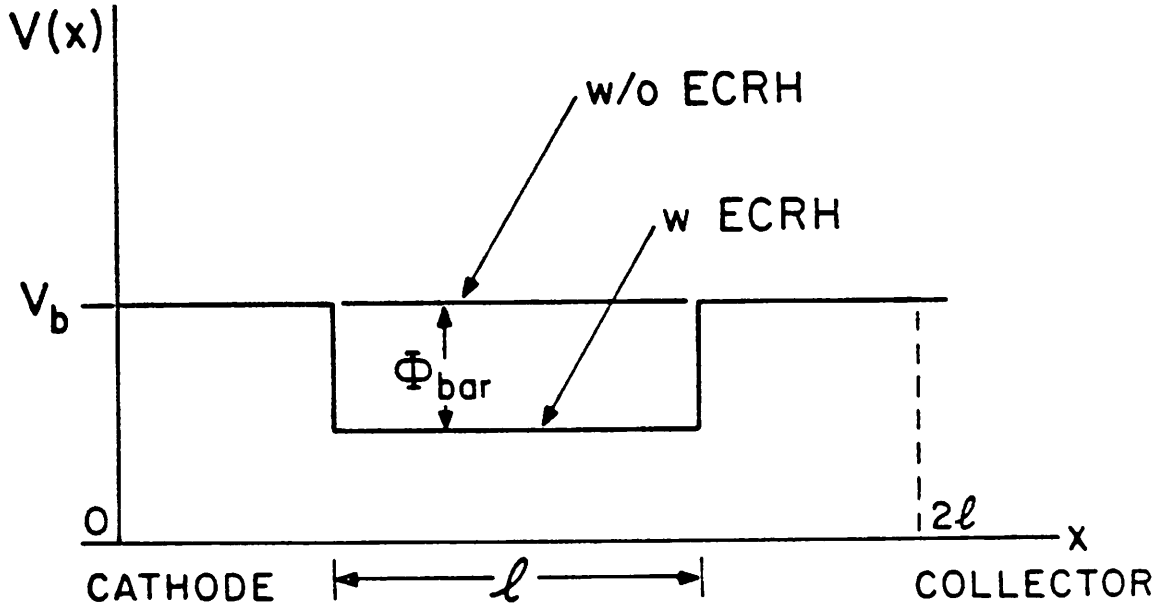
V(x)
w/o ECRH
w ECRH
V_b
Φ_{bar}
0
2ℓ
x
CATHODE
ℓ
COLLECTOR

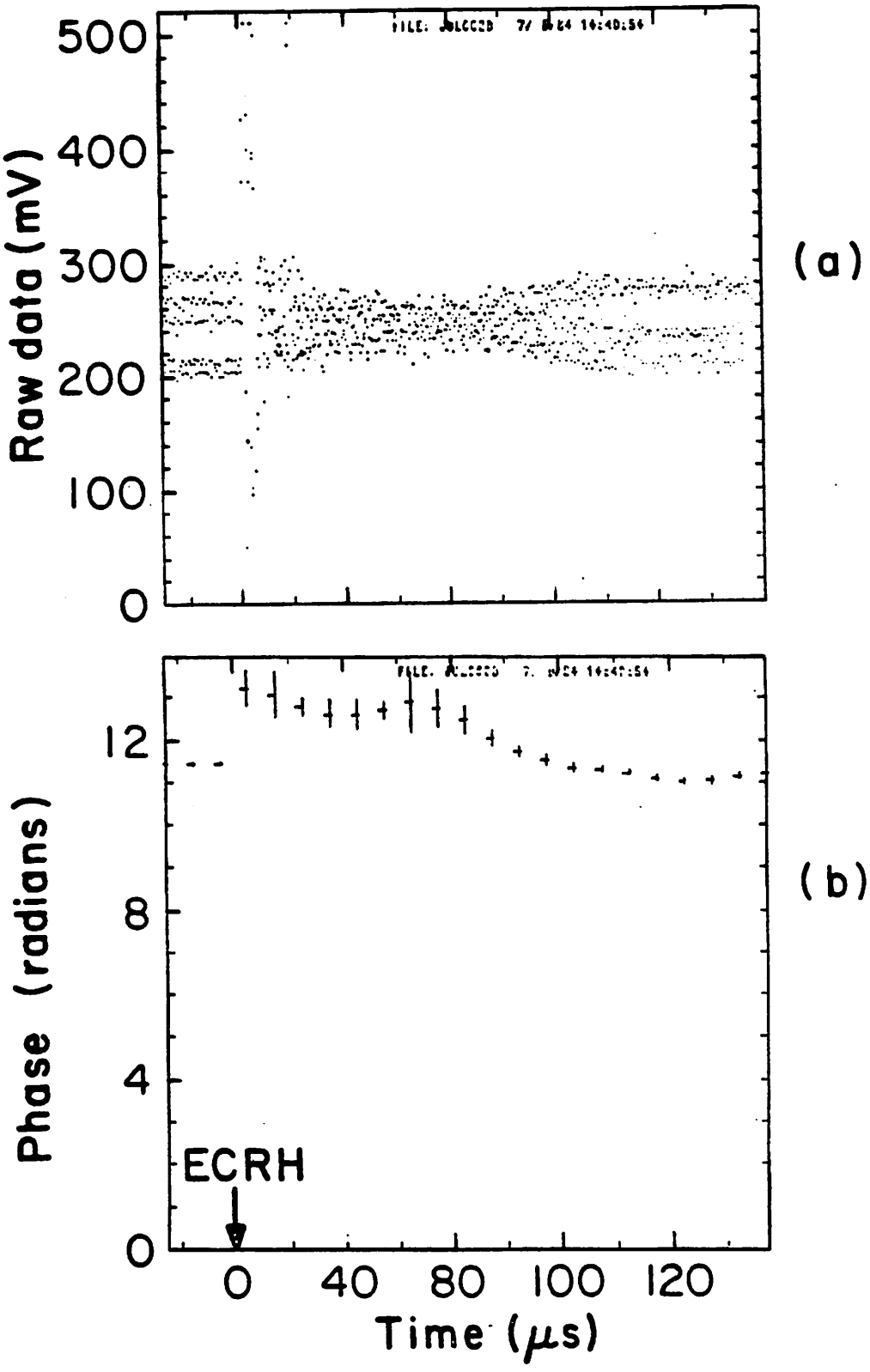
500
400
300
200
100
0
Raw data (mV)
(a)
12
8
4
0
Phase (radians)
ECRH
0
40
80
100
120
Time (μs)
(b)

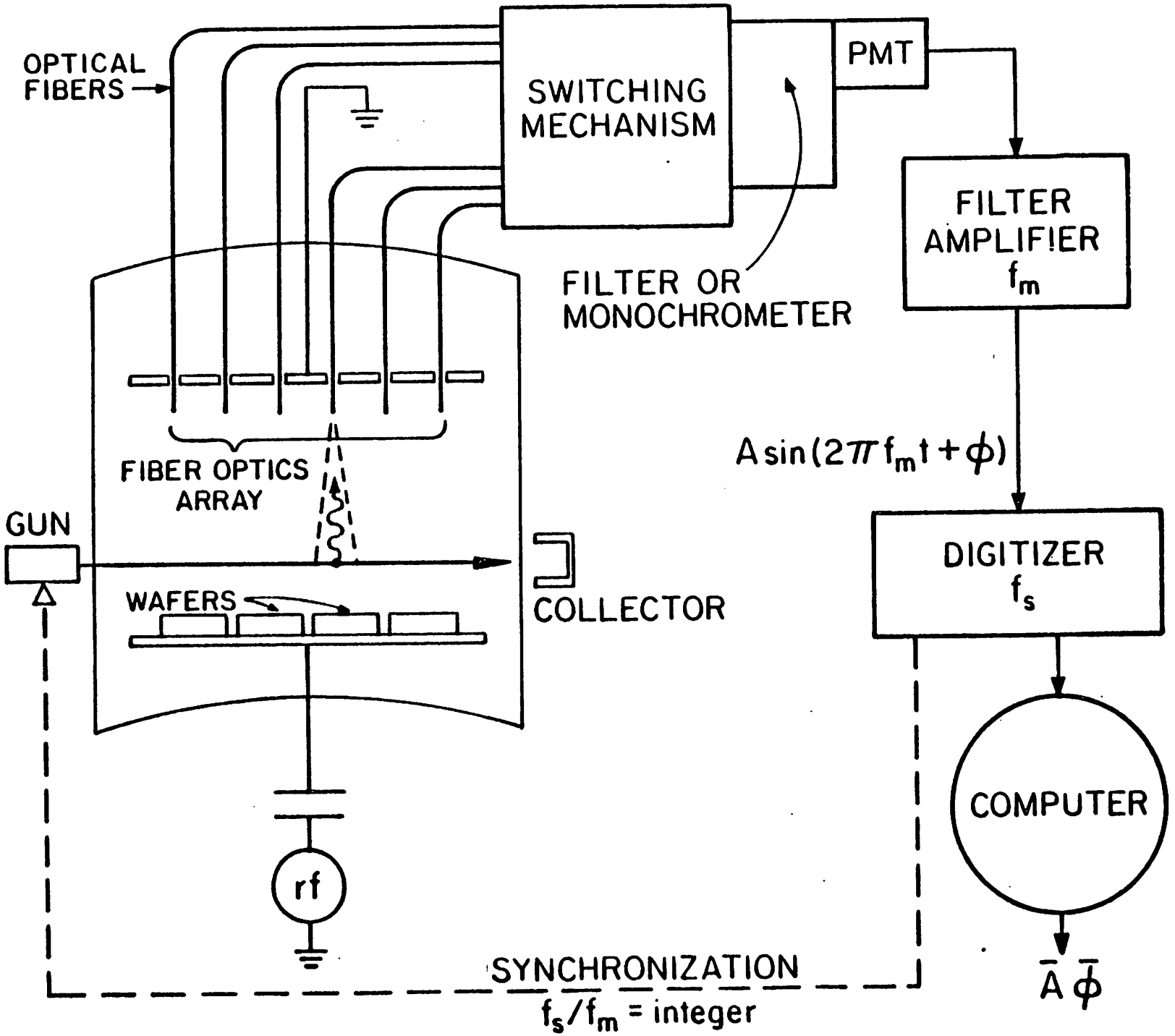
OPTICAL FIBERS
SWITCHING MECHANISM
PMT
FILTER OR MONOCHROMETER
FILTER AMPLIFIER f_m
$A\sin(2\pi f_m t + \phi)$
FIBER OPTICS ARRAY
GUN
WAFERS
COLLECTOR
DIGITIZER f_s
COMPUTER
rf
SYNCHRONIZATION
f_s/f_m = integer
$\bar{A}\,\bar{\phi}$

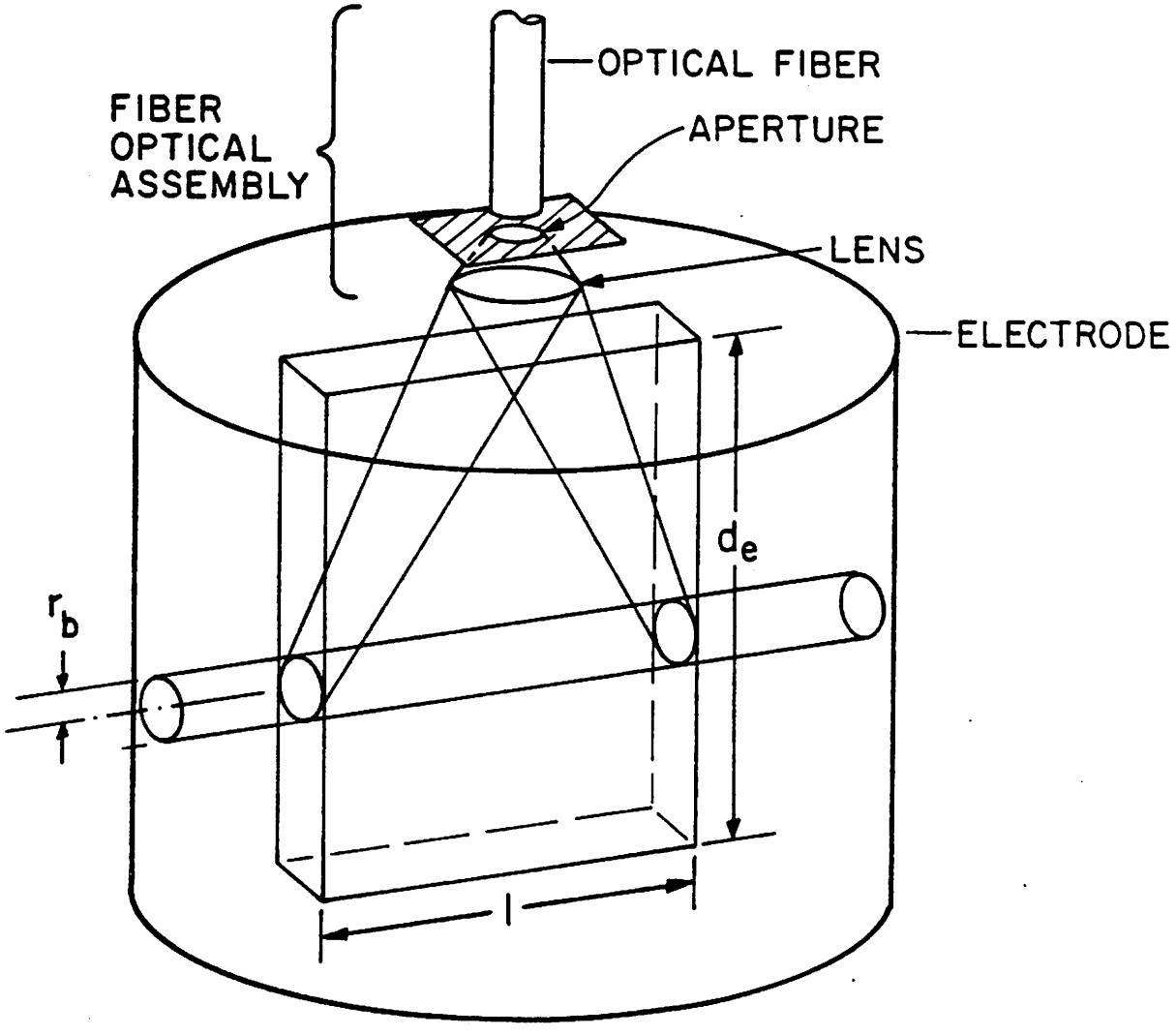
FIBER
OPTICAL
ASSEMBLY
OPTICAL FIBER
APERTURE
LENS
ELECTRODE
d_e
r_b
l

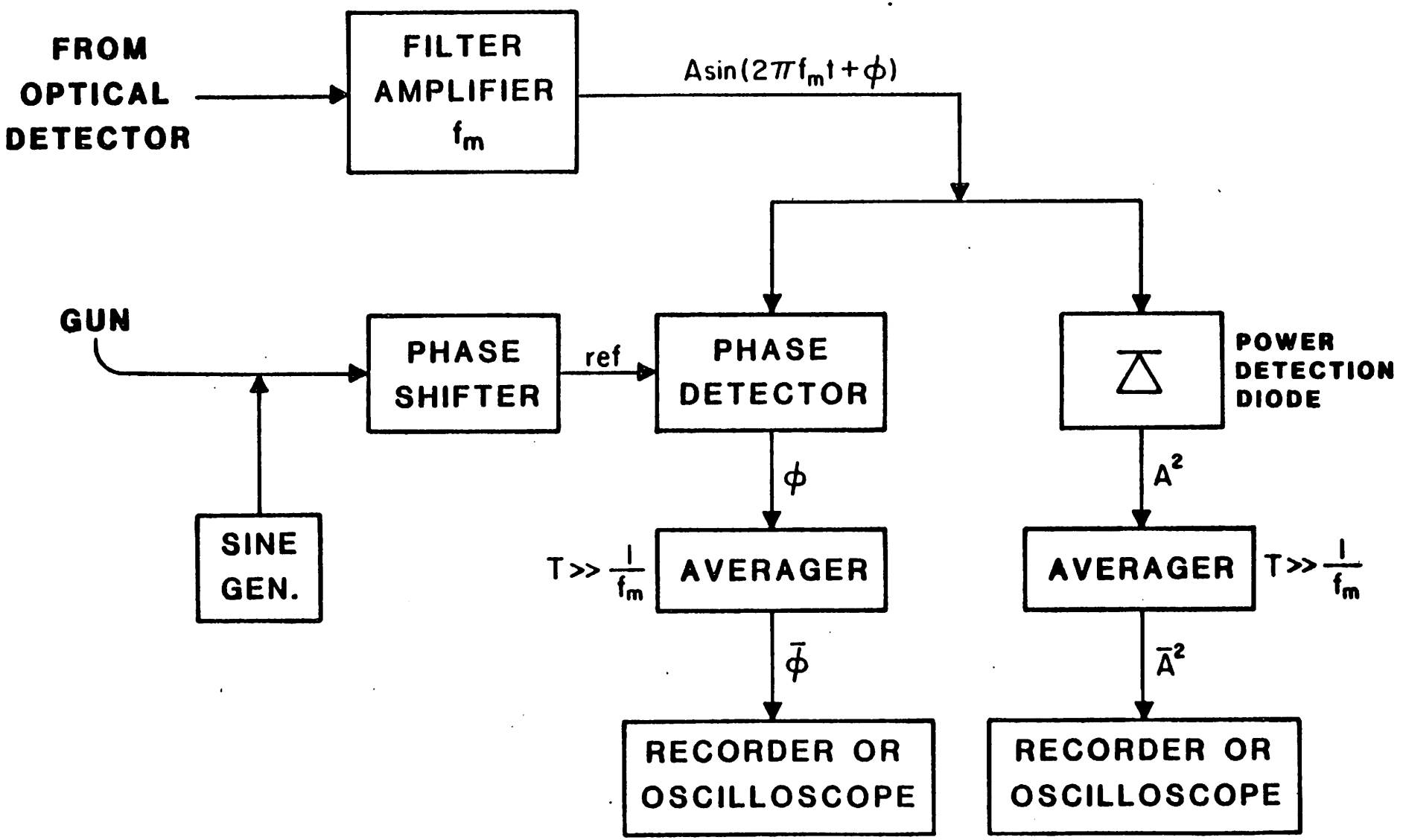
FROM OPTICAL DETECTOR
FILTER AMPLIFIER f_m
$A\sin(2\pi f_m t+\phi)$
GUN
PHASE SHIFTER
ref
PHASE DETECTOR
POWER DETECTION DIODE
SINE GEN.
ϕ
A^2
$T>>\frac{1}{f_m}$
AVERAGER
AVERAGER
$T>>\frac{1}{f_m}$
$\bar{\phi}$
$\bar{A}^2$
RECORDER OR OSCILLOSCOPE
RECORDER OR OSCILLOSCOPE

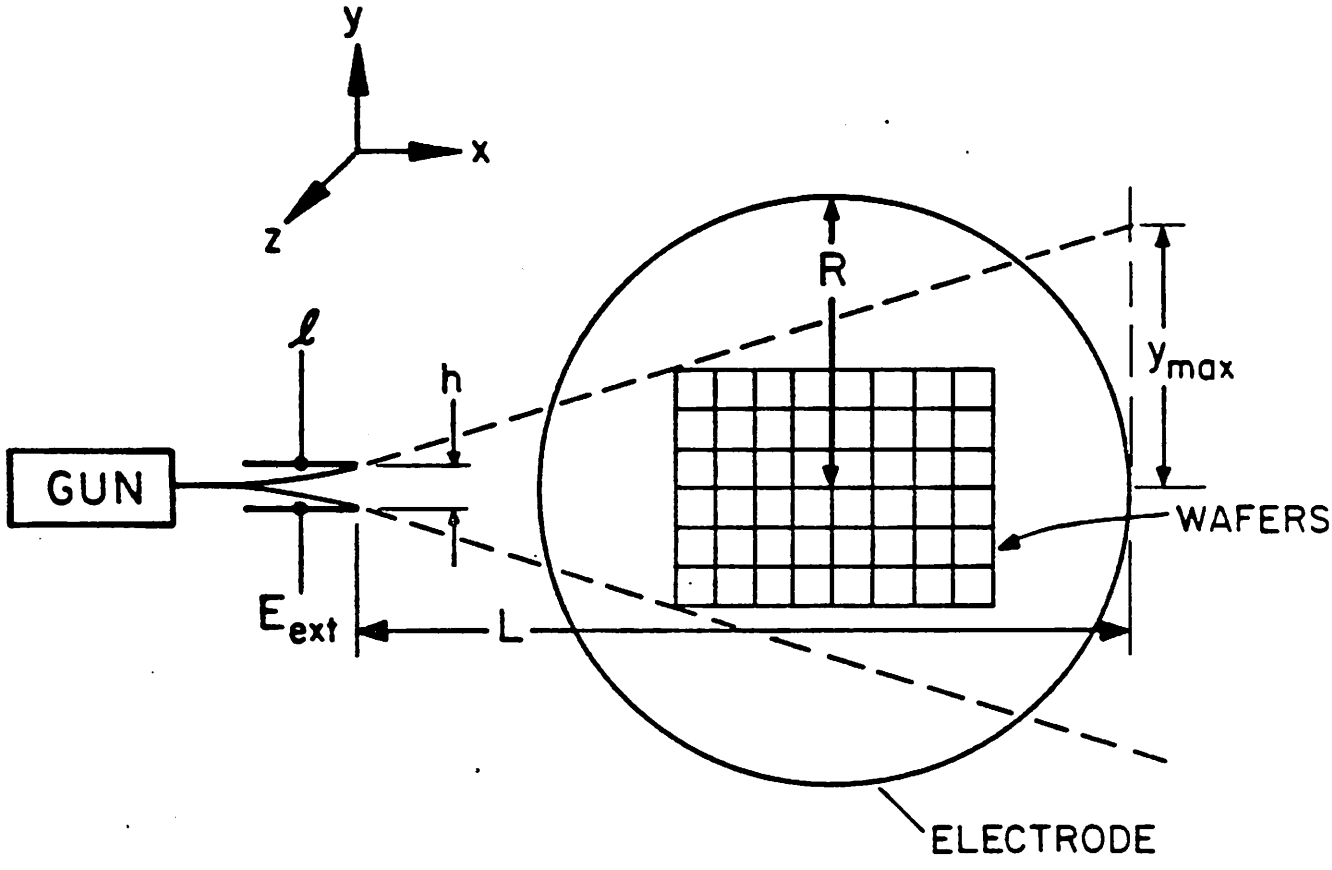
y
x
z
R
ℓ
h
y_{max}
GUN
WAFERS
E_{ext}
L
ELECTRODE

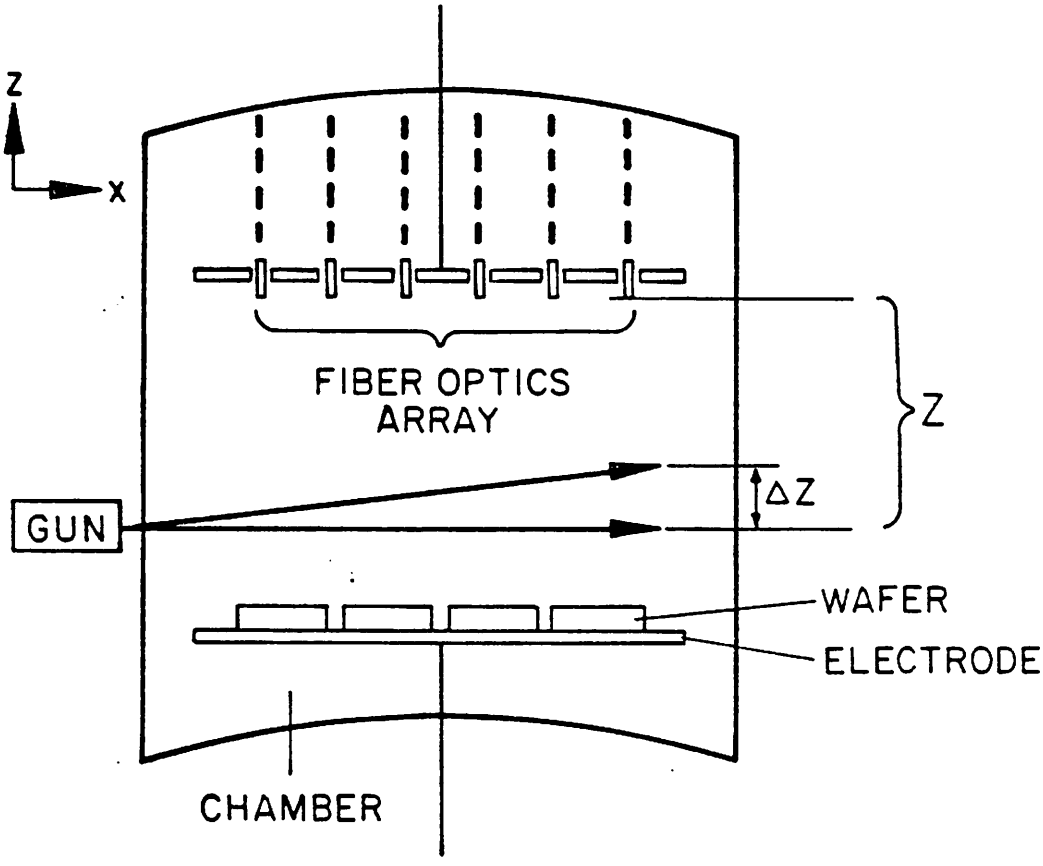
Z
X
FIBER OPTICS
ARRAY
Z
ΔZ
GUN
WAFER
ELECTRODE
CHAMBER